nanoenergy advances

MDPI

Article

Low-Temperature Solution Combustion-Synthesized CuSNanoparticulated Functional Thin Films: Structural and Optoelectronic Characterization Studies

Ioannis T. Papadas [1,*], Sergey M. Pozov [2], Iain Hamilton [3], Marc Sims [3], Ioannis Vamvasakis [4], Apostolos Ioakeimidis [2], Gerasimos S. Armatas [4], Donal D. C. Bradley [3,5,6] and Stelios A. Choulis [2]

1 Department of Public and Community Health, School of Public Health, University of West Attica, 11521 Athens, Greece
2 Molecular Electronics and Photonics Research Unit, Department of Mechanical Engineering and Materials Science and Engineering, Cyprus University of Technology, Limassol 3603, Cyprus; sm.pozov@gmail.com (S.M.P.); a.ioakeimidis@cut.ac.cy (A.I.); stelios.choulis@cut.ac.cy (S.A.C.)
3 Physical Science and Engineering Division, King Abdullah University of Science and Technology (KAUST), Thuwal 23955-6900, Saudi Arabia; iain.hamilton15@gmail.com (I.H.); smiscram@gmail.com (M.S.); donal.bradley@neom.com (D.D.C.B.)
4 Department of Materials Science and Engineering, University of Crete, 71003 Heraklion, Greece; jvamvasakis@gmail.com (I.V.); garmatas@materials.uoc.gr (G.S.A.)
5 Clarendon Laboratory, Department of Physics, University of Oxford, Oxford OX1 3PU, UK
6 NEOM Education, Research, and Innovation Foundation, NEOM University, Al Khuraybah 49643-9136, Saudi Arabia
* Correspondence: ipapadas@uniwa.gr

Abstract: In this paper, we present a one-step low-temperature solution combustion synthesis (SCS) of CuS nanoparticulated functional films processed via a simple blade-coating technique. This SCS route uses thiourea as a fuel and sulfur source, combined with copper(II) nitrate as an oxidant and a cupric ion source in an aprotic solvent such as non-toxic DMSO. It is hereby shown that the proposed SCS process formed a stable and completely dissolved molecular ink of thiourea and copper ion complexes, crucial for obtaining the pure crystalline phase of CuS nanoparticles (NPs). The CuS was formed by calcination at a low temperature of 200 °C during a brief annealing time of 20 min, to promote the synthesis of ~10 nm CuS NPs. The obtained CuS NPs were thoroughly analyzed in terms of structure and optoelectronic properties using various analytic and spectroscopic techniques, including TGA, XRD, FE-SEM, EDS, AFM, and four-point probe electrical resistivity measurements. The functionality of the prepared CuS nanoparticulated interlayers was evaluated by incorporating them as a hole injection layer (HIL) in Super Yellow (SY) organic light-emitting diodes (OLEDs).

Keywords: metal chalcogenides; CuS; covellite; copper sulfide; solution combustion synthesis; p-type semiconductor; hole injection layer; organic light-emitting diodes

Academic Editor: Mingyang Wei

Received: 30 November 2024
Revised: 9 February 2025
Accepted: 11 February 2025
Published: 18 February 2025

Citation: Papadas, I.T.; Pozov, S.M.; Hamilton, I.; Sims, M.; Vamvasakis, I.; Ioakeimidis, A.; Armatas, G.S.; Bradley, D.D.C.; Choulis, S.A. Low-Temperature Solution Combustion-Synthesized CuSNanoparticulated Functional Thin Films: Structural and Optoelectronic Characterization Studies. *Nanoenergy Adv.* **2025**, *5*, 3. https://doi.org/10.3390/nanoenergyadv5010003

1. Introduction

Transition metal chalcogenides (TMCs) are a vast representation of a category of inorganic materials that have attracted immense research interest due to their many technological applications [1,2]. TMCs have a stronger covalent bond than the corresponding metal oxides. This is related to the lower electronegativity values from oxygen (3.5) to sulfur (2.5), which can indicate that their covalent bonding character, as observed in their crystal structures and physicochemical and optoelectronic properties, has diverse functions

and applications [1,3]. TMCs such as NiS, ZnS, CoS, CdS, and CuS have already been applied in electrochemical applications, including photo- and electrocatalysis, gas sensors, and photovoltaic cells [4–8]. Among TMCs, copper sulfide (CuS) is one of the most significant metal chalcogenides, attracting a lot of attention in contemporary research due to its fascinating electronic properties [2,9,10].

Copper chalcogenides are binary compounds with a basic chemical formula of $Cu_{2-x}S$, ($0 \leq x \leq 1$), presenting different crystalline phases ranging from orthogonal to hexagonal, with a variety of stoichiometries, such as Cu_2S, $Cu_{1.95}S$, $Cu_{1.8}S$, $Cu_{1.75}S$, and CuS, which are known as thermodynamically stable structures at room temperature [3,9,11,12]. Additionally, the different stoichiometry and morphology of the above chemical formula shift the energy band gap, ranging from E_g~1.2 eV for Cu_2S to E_g~2.4 eV for CuS, affecting the optoelectronic properties [13].

CuS is an enticing material because of its Earth-abundant constituent elements, nontoxicity, low cost, and promising implementations in areas such as optoelectronic, photoconductive, and photothermal applications, thus making it a very popular choice among researchers [10,14–17]. CuS is a p-type semiconductor gaining major interest because of its metallic-like electrical conductivity, which is credited to free holes of copper vacancies. CuS has a broad range of implementations in lithium-ion batteries, solar cells, superconductors, gas sensors, optical filters, photothermal therapy, biosensors, drug delivery, antibiotic and antibacterial applications [7,9,18–41]. Regarding the applications stated above, a lot of work has been devoted to the synthesis of CuS with a variety of shapes and sizes such as nanowires, nanorods, nanoplates, nanotubes, and nanoflakes [11,42–46]. Many synthetic paths, such as the solid-state reaction in high-vacuum conditions, the reflux method, electrodeposition, sulfurization reactions, liquid–liquid interface, and hydro/solvothermal and co-precipitation methods, have been reported for the synthesis of CuS nanostructures [10,14,42–44,47–50]. However, the production of high-purity and monodisperse nanoparticles (NPs) remains a significant challenge that has not yet been overcome.

Organic light-emitting diodes (OLEDs) are thin-film devices that exhibit highly efficient emission from a large 2D surface plane, in contrast to traditional LEDs, which, although also efficient, tend to be point sources. OLEDs have a wide range of commercial applications, including solid-state lighting and display technologies [51–54]. Poly(3,4-ethylenedioxythiophene)-poly(styrene sulfonate) (PEDOT:PSS) is a conducting hole injection layer (HIL) polymer that is most frequently used in the normal architecture of OLEDs due to its low toxicity, wide availability, ease with which it can be processed from a solution, and moderately high work function [55,56]. However, the hygroscopic and acidic nature of PEDOT:PSS leads to degradation issues, weathering the ITO contacts and eventually decreasing the stability of OLEDs [57–60]. Another well-known solution-processible HIL, namely graphene oxide, exhibits low electrical conductivity and low hole injection efficiency [13,61]. As a result, developing alternative p-type semiconductor HILs that would display high electrical conductivity and resistance to chemicals and moisture remains an open challenge.

In this paper, we aim to show an attractive method of low-temperature solution combustion that leads to CuS nanoparticulated functional thin films. This process utilizes thiourea as a fuel and sulfur source, alongside nitrate as the oxidizer agent in DMSO solvent. In our study, CuS NPs of an average diameter of ~10 nm were synthesized utilizing a low-cost and efficient solution combustion synthesis process. The synthesized CuS NPs were formed by calcination at a low temperature of 200 °C during a time frame of 20 min. The as-obtained CuS NPs were thoroughly analyzed for their structure and optoelectronic properties using various techniques, including TGA, XRD, FE-SEM, EDS, AFM, and four-point probe electrical resistivity measurements. The results demonstrate

that the prepared CuS films have a highly pure crystalline structure with high electrical conductivity. Moreover, the suggested synthetic route facilitates the formation of compact films with low roughness through the blade-coating technique, which is suitable for the fabrication of large printed electronic devices. In addition, CuS NPs are hereby used for the first time as hole injection layers (HILs) built in Super Yellow (SY) OLEDs, and the primary results of this device's performance are illustrated in this paper.

2. Materials and Methods

2.1. Materials

Pre-patterned glass-ITO substrates (sheet resistance 4 Ω/sq) were purchased from Psiotec Ltd. (Berkhamsted, UK). Solution-processable poly(p-phenylene vinylene) PPV-based polymer, PDY-132 Livilux® Super Yellow (SY), were purchased from Merck (Darmstadt, Germany) and used as a light-emissive polymer layer. SY was dissolved inside an inert glovebox atmosphere using toluene solvent at a 6.5 mg/mL concentration. All the other chemicals used in this study were purchased from Sigma-Aldrich (St. Louis, MO, USA).

2.2. Synthesis of CuS NP Films

Following the typical synthesis of CuS nanoparticulated functional films, 1 mmol of copper(II) nitrate trihydrate and 2 mmol of thiourea were dissolved in 10 mL of DMSO under stirring for 30 min at room temperature. The resulting mixture was then filtered through a 0.22 μm pore diameter polyvinylidene difluoride (PVDF) filter before further processing. The resulting solution was diluted in DMSO at a 13 mg/mL concentration and utilized as a coating ink on the ITO substrates with the doctor blade technique; then, the created films were dried for 10 min at 100 °C on a preheated plate. Subsequently, both the contact points of the ITO substrates and the non-patterned glass area of the substrate were cleaned carefully using a cotton swab moistened with deionized water,thus avoiding a short-circuit whilst achieving a functional area of 9 mm^2. The resulting films were calcinated in a preheated oven at 200 °C under ambient air for 20 min to complete the combustion process. Following this, the films were allowed to settle at room temperature. The final thin CuS film thickness was ~45 nm.

2.3. Device Fabrication

The fabrication of a basic organic light-emitting diode structure (ITO/CuS/SY/LiF/Al) utilized the CuS NP films, prepared on ITO substrates as described above, with the desired property of a hole injection layer. The ITO substrates had been previously cleaned in acetone and isopropanol under sonication for about 10 min, then dried at room temperature, and set under a UV-ozone treatment for 5 min. A highly concentrated Super Yellow/toluene solution was spin-coated at 6000 rpm for 30 s in an inert glovebox atmosphere directly onto the CuS-coated ITO substrate. The resulting Super Yellow films, annealed in the same inert atmosphere on a hotplate at 50 °C for 20 min, yielded a thickness of around ~80 nm. Thereafter, the contact points with the ITO substrates and the non-patterned glass area were meticulously cleaned with a cotton swab saturated with chlorobenzene (CB).To finalize the OLED stack, 1 nm (0.2 A/s) of lithium fluoride (LiF) and 100 nm (2 A/s) of aluminum (Al) were thermally evaporated in a vacuum chamber (Angstrom Engineering, Kitchener, ON, Canada) at a minimum pressure of ~2×10^{-6} mbar through a shadow mask to achieve a functional area of 9 mm^2. Finally, the fabricated devices were encapsulated by placing them on a glass slide, with an Ossila E131 (Sheffield, UK) epoxy resin, which was activated by 365 nm UV irradiation.

2.4. Characterization

Thermogravimetric analysis (TGA) measurements were performed on a Perkin-ElmerDiamond system. Thermal analysis was conducted from 40 to 400 °C under an air atmosphere (100 mL min^{-1} flow rate) with a heating rate of 10 °C min^{-1}. X-ray diffraction (XRD) patterns were collected on a PANanalyticalX'pert Pro MPD powder diffractometer (40 kV, 45 mA) using CuKα radiation (λ = 1.5418 Å), (Malvern Panalytical, Worcestershire, UK). Energy-dispersive X-ray spectroscopy (EDS) and field emission electron microscopy (FE-SEM) were carried out using a JEOL JSM-IT700HR microscope equipped with a JED-2300 detector (JEOL Ltd., Tokyo, Japan). EDS data acquisition was carried out at least ten times (at different locations) for each sample using an accelerating voltage of 20 kV and a 60 s accumulation time. Diffuse reflectance UV-Vis spectra were recorded at room temperature with a UV-2600 optical spectrophotometer (Shimadzu, Kyoto, Japan), using powder $BaSO_4$ as a 100% reflectance standard. Reflectance data were converted to absorption (α/S) data according to the Kubelka–Munk equation [62]: $\alpha/S = (1-R)^2/(2R)$, where R is the reflectance and α and S are the absorption and scattering coefficients, respectively. The energy band gap (E_g) values of the samples were determined from Tauc plots for direct allowed transitions, i.e., the plot of $(\alpha h\nu)^2$ vs. photon energy ($h\nu$), where α is the absorption coefficient and $h\nu$ is the energy of incident photons. AFM images were obtained using an AFM EasyScan 2 controller under the tapping mode (Nanosurf, Switzerland). The thickness of the films was measured with a Dektak 150 profilometer (Veeco, NY, USA). Photoelectron spectroscopy in air (PESA) measurements were recorded using a PESA spectrometer, Model AC-2 and a power number of 0.3 (RikenKeiki, Tokyo, Japan). Finally, the completed devices were characterized using current density-voltage-luminance characteristics (JVL), obtained using a Botest LIV functionality test system with a calibrated silicon photodiode sensor (spectral sensitivity 350–730 nm and responsivity 60 nA/lux). All the characterizations were performed under ambient conditions.

3. Results and Discussion

SCS has been recently implemented in the production of metal oxide thin films at low temperatures [63–65]. Overall, SCS exhibits the benefit of efficiently synthesizing uniform materials featuring a fine particle size and, notably, at a considerably lower temperature, compared to traditional solid-state reaction processes and co-precipitation, sol–gel, and hydrothermal synthesis methodologies. During SCS, the quantity and nature of chemical compounds, such as the fuel and oxidizing agent, have a significant impact on the morphological and structural properties of the resulting materials [6,64]. In addition, the selection of the fuel reagent and solvents for the solution combustion process is critical in preventing the development of large clusters and precipitations [66].

In this study, for the first time, we used an aprotic polar solvent, such as non-toxic DMSO, to form a stable and entirely dissolved molecular ink of thiourea and copper ion complexes. Dissolved thiourea in DMSO was employed as a fuel and sulfur source, while nitrates (copper nitrate) served as an oxidizing agent. This was critically important for obtaining uniform crystalline-phase of CuS NPs. DMSO as an aprotic polar solvent has an exceptionally high pKa and does not possess a reactive oxygen nature, unlike protic polar solvents such as H_2O and ROH [67,68]. Thus, by utilizing DMSO solvent, the formation of Me–O–Me and/or Me–O–C chemical bonds was prevented [69,70]. This formation can result in precipitation and a change in bulk solution composition, creating impurities in the final material, as well as mixed crystal phases. Moreover, the advantage of using thiourea lies in its functions as a chelating ligand capable of solvating copper cations through the coordinated soft Lewis base S-donor site with the corresponding ions [71]. This process

generated pure single crystals of CuS NPs (see below), which subsequently formed a film composed of a continuous network of linked CuS NPs.

3.1. Synthesis and Characterization of CuS Nanoparticles

Thermogravimetric analysis (TGA) was used to observe the combustion reaction. The reaction was carried out in ambient air, using a heating rate of 10 °C min^{-1}. As depicted in Figure 1a, the reaction demonstrated a pronounced and steep mass loss at a temperature range of ~120–150 °C as seen in the TGA curve, credited to the formation of CuS by SCS. A secondary stage of mass loss appeared at around 300 °C, which was attributed to the oxidation of organic residues and the transformation of CuS to $CuSO_4$, as confirmed by XRD of the residual material calcinated at 300 °C (Figure S1) [72]. This suggests that the synthesis of CuS NPs by the combustion approach can efficiently occur at a significantly lower temperature.

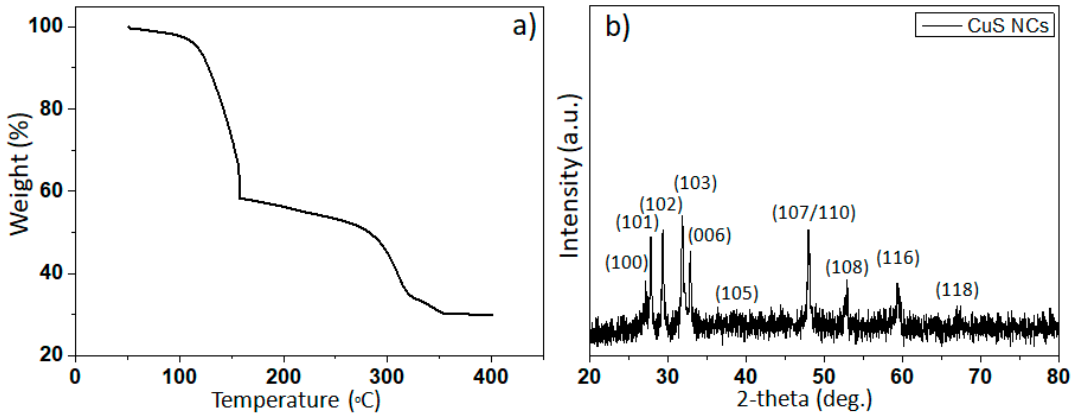

Figure 1. (**a**) TGA profile of the prepared CuS material via the combustion process. (**b**) Powder X-ray diffraction pattern of CuS nanocrystals (NCs) annealing at 200 °C for 20 min.

Figure 1b depicts the XRD pattern of the CuS nanocrystals synthesized at 200 °C for 20 min by SCS method. All the corresponding diffraction peaks confirmed the hexagonal covellite CuS crystal structure with lattice constants a = 3.792 Å and b = 16.34 Å (JCPDS No. 06-0464). No other crystalline phase, such as Cu_2S, $Cu_{1.8}S$, and $Cu_{1.96}S$, was noted, thus revealing the purity of the synthesized material [73]. The presence of broad diffractions stipulated the small grain composition of CuS; by applying the Scherrer's equation to the (102) diffraction peak, the mean grain size of the 200 °C annealed sample was calculated to be ~10 nm.

In order to evaluate the CuS morphology, field emission scanning electron microscopy (FE-SEM) was employed. The FE-SEM image depicted in Figure 2a confirms that CuS consists of spherical nanoparticles with an average size of ~10 nm. The SEM-EDS elemental mapping depicted in Figure 2b,c reveals a homogeneous distribution of Cu and S elements throughout the CuS material, suggesting a uniform composition for all CuS NPs. The EDS analysis showed that the average atomic ratio of Cu to S was 1:1 (Figure S2).

The inset in Figure 3a displays the UV-Vis/NIR absorption spectrum of the CuS NPs. CuS NPs exhibited a pronounced optical absorption onset in the visible region at a wavelength of approximately 510 nm. This absorption was associated with an energy band gap (E_g) of 2.44 eV, according to the corresponding Tauc plot for direct allowed transition, i.e., $(\alpha h\nu)^2$ vs. photon energy plot (Figure 3a). The E_g of CuS NPs was similar to other reported values of CuS materials synthesized at the nanoscale that show a slight blue shift in comparison to corresponding bulk material (E_g~2.4 eV), possibly related to quantum confinement effects [10]. The absorption tail at longer wavelengths arose from

scattering effects and/or inter-band transitions from the valence band to mid-gap states in the CuS nanoparticles [74,75]. Figure 3b shows the photoelectron spectroscopy in air (PESA) measurement data of the photocurrent yield$^{0.3}$ against the photon energy of a CuS NP film. The intersection of the linear line of best fit (red dashed line) after photoelectron emission onset with the baseline (blue dashed line) gave the value of the CuS ionization energy (IE), ~4.9 eV [76].

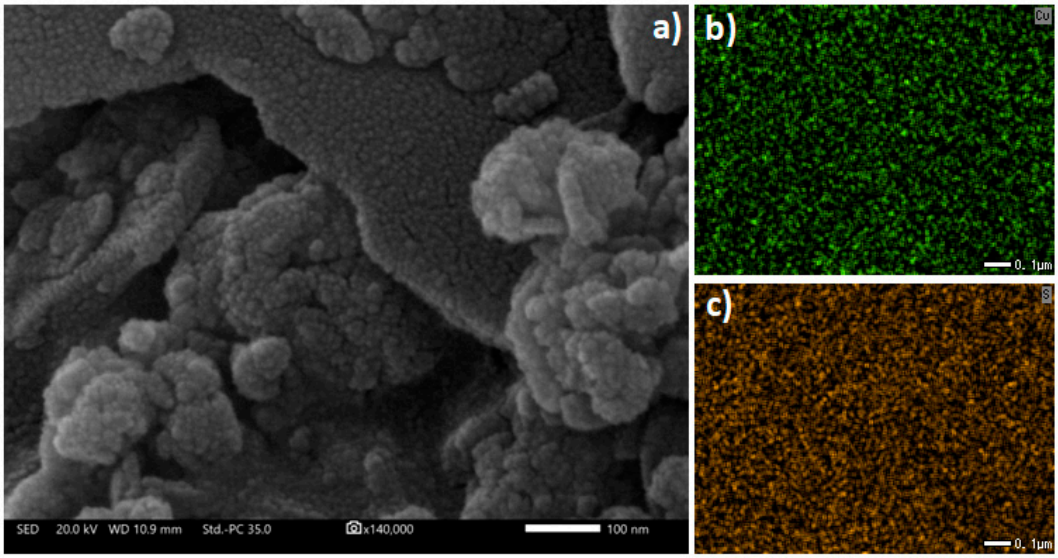

Figure 2. (**a**) Typical FE-SEM image and (**b**,**c**) EDS element mapping images of as-prepared CuS NPs. Cu element (green color) and S element (orange color).

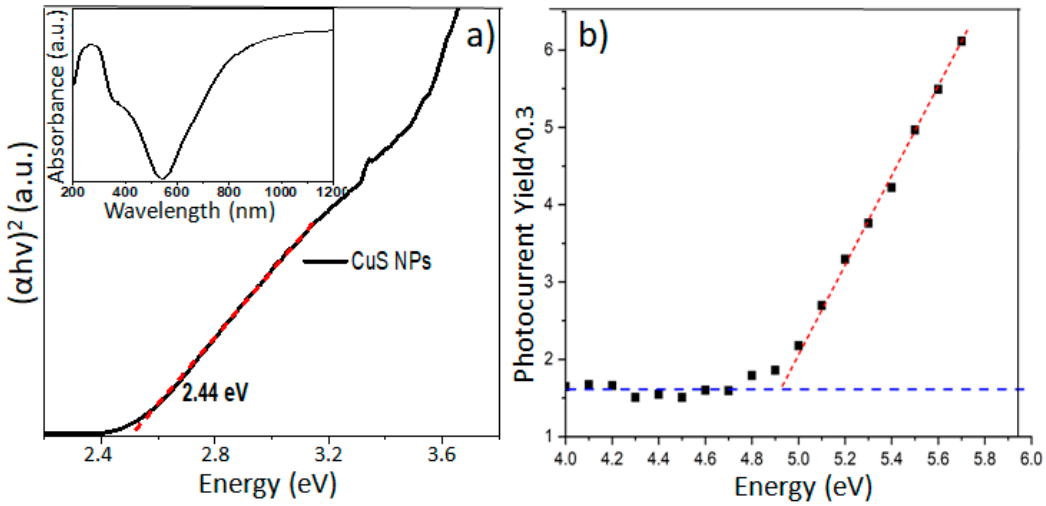

Figure 3. (**a**) Tauc plot $(\alpha hv)^2$ vs. photon energy (hv), showing an energy band gap of 2.44 eV for the synthesized CuS NPs. The inset depicts the UV-Vis/NIR absorption spectrum of CuS NPs. (**b**) PESA measurement results for a CuS NP film.

3.2. Blade-Coating-Processed Thin Films of CuS NPs

The blade-coating technique was employed to create thin films of CuS NPs on ITO substrates, utilizing the processing parameters outlined in the experimental section. Figure S3 displays the surface topography obtained by AFM for a 45 nm blade-coated film of CuS NPs on ITO-coated glass substrates. The CuS NP film revealed a smooth and dense topography of just 5.6 nm roughness. Producing a CuS layer with low surface roughness is advantageous for the performance of OLEDs because it enables the establishment of a uniform electric field across the active area of the device. Furthermore, the compacted

nanoparticulate CuS film demonstrated a significant elevation in electrical conductivity, providing a conductivity as high as 94.7 S cm^{-1} at room temperature as measured by the four-point probe electrical resistivity technique. The low surface roughness of the CuS nanoparticulated thin films (5.6 nm) together with the deep work function (4.9 eV) and the relatively high electrical conductivity (94.7 S cm^{-1}) qualified the SCS-based CuS thin film as a potentially good interlayer candidate for incorporation within organic optoelectronic device structures.

3.3. Device Performance

The functionality of CuS nanoparticulated interlayers is investigated by incorporating the as-synthesized CuS thin films as hole injection layers (HILs) in a Super Yellow (SY)-based, OLED structure, as presented in Figure 4a.

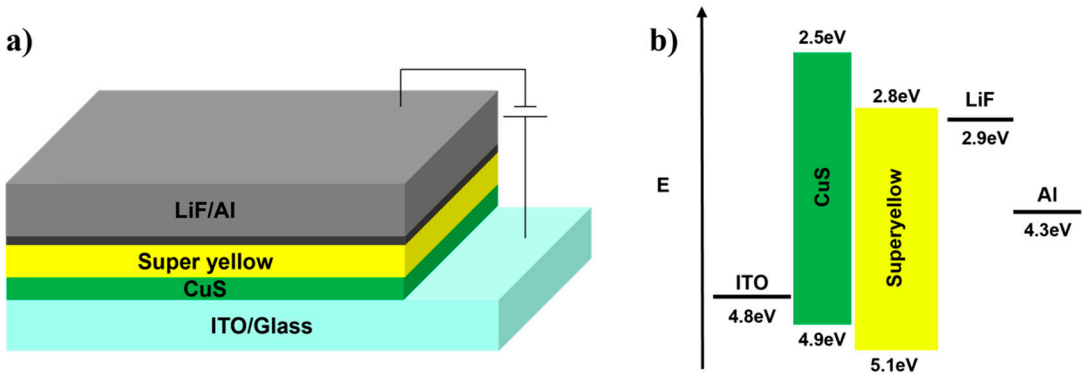

Figure 4. Schematic illustration of (**a**) normal SY:OLEDs (ITO/CuS/SY/LiF/Al) and (**b**) flat band diagram of the standard configuration of a Super Yellow OLED device.

Figure 5 shows the electroluminescent performance of the test SY:OLED structure using, for the first time, SCS-based CuS as an HIL. As shown in Figure 5a, SY:OLEDs incorporating CuSHIL exhibited a turn-on voltage of 2.6 V and a luminance of 10k cd/m^2. Figure 5b presents the JV characteristics. The SY:OLED CuSHIL displayed a current efficiency (CE) and power efficacy (PE) of up to 2.7 cd/A and 1.9 lm/W, respectively, as presented in Figure 5c,d. Both the CE and PE curves peaked in the range of 100–1000 cd/m^2. While these preliminary results for SY:OLEDs with CuS as a novel HIL confirmed the successful functionality of SCS-based CuS NP interlayers in a simple, non-thickness-optimized OLED stack, the obtained SY:OLED efficiency was lower than that typically achieved (usually 5.0 cd/A and 4.5 lm/W) for optimized PEDOT:PSS HIL-based SY:OLEDs [56]. Given the difference in HIL work functions (CuS vs. PEDOT:PSS, 4.9 eV vs. 5.1 eV, respectively), experimentally verified by the presented (Figure 3b) PESA measurements and schematically illustrated in Figure 4b, the lower performance of CuS HIL-based SY:OLEDs compared to PEDOT:PSS HIL-based SY:OLEDs likely stemmed from differences in the nature of the CuS | SY interface vs. the PEDOT:PSS | SY interface. In Figure S4, the CuS HIL device appears more injection-limited (note the very gradual slope in log (I) versus voltage compared to the very abrupt slope that would be expected from a device with current flow that is limited by space charge effects) compared to the PEDOT:PSS-based HIL device. The energetic offset between the HOMO levels of CuS and SY may have contributed to reducing the efficacy of hole injection, although, at 0.2 eV, the barrier was relatively small, not fully explaining the strong injection-limited characteristics. The lower performance of the SY:OLED device may be attributable to a number of factors, but it is not possible to pinpoint the exact cause(s) without further studies. One direction of investigation would stem from the expectation that CuS films are optically quite dense, so the calculation of an optimal interlayer thickness may be necessary to improve light outcoupling efficiency.

Besides purely optical considerations, the relative electronic characteristics of the CuS | SY interface vs. the PEDOT:PSS | SY interface likely play a somewhat significant role given the small difference in HIL work functions (CuS vs. PEDOT:PSS, 4.9 eV vs. 5.1 eV, respectively) [56]. The CuS:SY interface is likely more injection-limited compared to the PEDOT:PSS | SY interface, so recombination profiles are affected accordingly. Explicitly, this distinction would naturally pull the recombination zone closer to the interlayer in the case of CuS, which, in turn, would also affect the light outcoupling efficiency, depending on the ITO (230 nm) | IL (45 nm) | SY (80 nm) cavity constraint. Nevertheless, we have hereby demonstrated that the work function of CuS is adequately aligned to the HOMO level of SY to produce a working OLED and that optimization could very feasibly improve the device's characteristics.

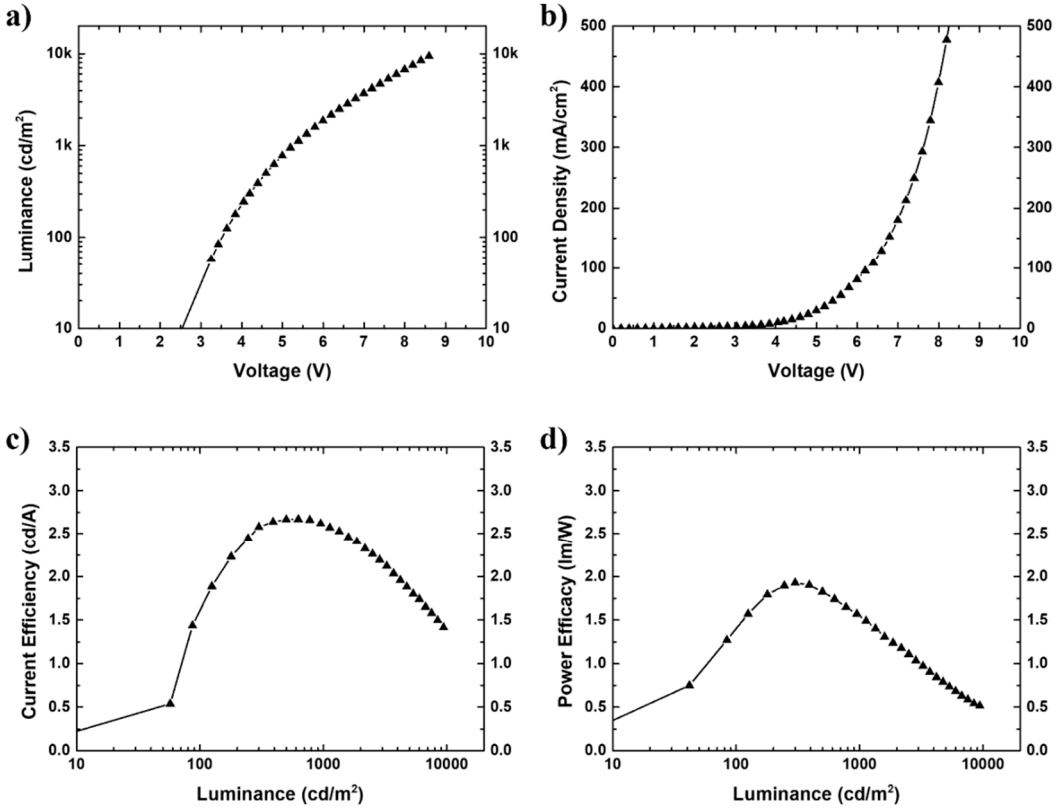

Figure 5. Electroluminescent performance of OLED devices based on the ITO/CuS/SY/LiF/Al device structure: (**a**) luminance-voltage characteristics (LV), (**b**) current density-voltage (JV) characteristics, (**c**) current efficiency as a function of luminance, and (**d**) power efficacy as a function of luminance.

4. Conclusions

To conclude, SCS at a low temperature, employing thiourea as a fuel and sulfur source, was effectively developed and implemented to fabricate functional and uniform nanoparticulated CuS thin electronic films. The formation of monodispersed CuS NPs with a size of ~10 nm was entirely controlled, utilizing thiourea as the chelating agent, which was completely dissolved in an aprotic environmentally friendly solvent like DMSO. The SCS process occurred at a relatively low temperature of 200 °C with a brief reaction time of 20 min, leading to high-quality and compact nanoparticulated CuS films with a low roughness of ~5.6 nm, a work function of 4.9 eV, and an exceptionally high electrical conductivity of ~94.7 S cm^{-1} for solution-processed nanoparticulated HIL. The presented X-ray diffraction, EDS, and FE-SEM measurements validated the pure crystalline phase and small-particle composition of the SCS-based CuS. Moreover, the proposed SCS route enabled the fabrication of electronic films utilizing the blade-coating processing technique,

suitable for the fabrication of up-scalable printed electrical devices. The functionality of SCS-based CuS nanoparticulated interlayers was confirmed by their incorporation as HIL in SY:OLEDs. The reported SCS method offers a pathway to fabricate solution-processed metal chalcogenides at the nanoscale that can be used as functional materials for future advanced electronic applications.

Supplementary Materials: The following supporting information can be downloaded at https://www.mdpi.com/article/10.3390/nanoenergyadv5010003/s1, Figure S1: XRD pattern of precursors materials calcinated at a temperature of 300 °C for 20 min; Figure S2: EDS spectrum for CuS NPs; Figure S3: AFM image of ITO/CuS NP thin films after combustion synthesis at 200 °C for 20 min; Figure S4: J-V characteristics (log scale) of OLED devices based on the ITO/CuS/SY/LiF/Al device structure.

Author Contributions: Conceptualization, I.T.P., D.D.C.B. and S.A.C.; data curation, I.T.P., S.M.P., I.H., M.S., I.V., A.I. and G.S.A.; formal analysis, I.T.P., S.M.P., I.H., M.S., I.V., A.I., G.S.A., D.D.C.B. and S.A.C.; funding acquisition, S.A.C.; investigation, I.T.P. and S.M.P.; methodology, I.T.P., S.M.P., I.H., M.S., G.S.A., D.D.C.B. and S.A.C.; supervision, I.T.P., G.S.A., D.D.C.B. and S.A.C.; visualization, S.A.C.; writing—original draft, I.T.P., S.M.P., I.H., M.S. and S.A.C.; and writing—review and editing, I.T.P., S.M.P., I.H., M.S., I.V., A.I., G.S.A., D.D.C.B. and S.A.C. All authors have read and agreed to the published version of the manuscript.

Funding: This research received no external funding.

Data Availability Statement: All relevant data are within the paper.

Conflicts of Interest: The authors declare no conflicts of interest.

References

1. Coughlan, C.; Ibáñez, M.; Dobrozhan, O.; Singh, A.; Cabot, A.; Ryan, K.M. Compound Copper Chalcogenide Nanocrystals. *Chem. Rev.* **2017**, *117*, 5865–6109. [CrossRef] [PubMed]
2. Shamraiz, U.; Hussain, R.A.; Badshah, A. Fabrication and Applications of Copper Sulfide (CuS) Nanostructures. *J. Solid State Chem.* **2016**, *238*, 25–40. [CrossRef]
3. Masar, M.; Urbanek, M.; Urbanek, P.; Machovska, Z.; Maslik, J.; Yadav, R.S.; Skoda, D.; Machovsky, M.; Kuritka, I. Synthesis, Characterization and Examination of Photocatalytic Performance of Hexagonal Covellite CuS Nanoplates. *Mater. Chem. Phys.* **2019**, *237*, 121823. [CrossRef]
4. Kaur, M.; Nagaraja, C.M. Template-Free Synthesis of ZnS Nanocrystals with a New Sulfur Source and Their Photocatalytic Study. *Mater. Lett.* **2015**, *154*, 90–93. [CrossRef]
5. Arunkumar, S.; Tamilselvan, S.; Ashokkumar, T.; Geetha, R.; Govindaraju, K.; Ganesh Kumar, V.; Singaravelu, G.; Vijai Anand, K. One-Pot Room Temperature Novel Synthesis of Water-Soluble CdS Nanotriangles via Green Route. *Mater. Lett.* **2014**, *134*, 225–228. [CrossRef]
6. Papadas, I.T.; Ioakeimidis, A.; Vamvasakis, I.; Eleftheriou, P.; Armatas, G.S.; Choulis, S.A. All-Inorganic p−n Heterojunction Solar Cells by Solution Combustion Synthesis Using N-Type $FeMnO_3$ Perovskite Photoactive Layer. *Front. Chem.* **2021**, *9*, 754487. [CrossRef] [PubMed]
7. Chen, X.; Yang, J.; Wu, T.; Li, L.; Luo, W.; Jiang, W.; Wang, L. Nanostructured Binary Copper Chalcogenides: Synthesis Strategies and Common Applications. *Nanoscale* **2018**, *10*, 15130–15163. [CrossRef] [PubMed]
8. Vamvasakis, I.; Andreou, E.K.; Armatas, G.S. Mesoporous Dual-Semiconductor ZnS/CdS Nanocomposites as Efficient Visible Light Photocatalysts for Hydrogen Generation. *Nanomaterials* **2023**, *13*, 2426. [CrossRef]
9. Wang, K.; Tan, G. Synthesis and Optical Properties of CuS Nanocrystals by Mechanical Alloying Process. *Curr. Nanosci.* **2010**, *6*, 163–168. [CrossRef]
10. Pejjai, B.; Reddivari, M.; Kotte, T.R.R. Phase Controllable Synthesis of CuS Nanoparticles by Chemical Co-Precipitation Method: Effect of Copper Precursors on the Properties of CuS. *Mater. Chem. Phys.* **2020**, *239*, 122030. [CrossRef]
11. Zeinodin, R.; Jamali-Sheini, F. In-Doped CuS Nanostructures: Ultrasonic Synthesis, Physical Properties, and Enhanced Photocatalytic Behavior. *Phys. B Condens. Matter* **2019**, *570*, 148–156. [CrossRef]
12. Safrani, T.; Jopp, J.; Golan, Y. A Comparative Study of the Structure and Optical Properties of Copper Sulfide Thin Films Chemically Deposited on Various Substrates. *RSC Adv.* **2013**, *3*, 23066–23074. [CrossRef]

13. Woods-Robinson, R.; Han, Y.; Zhang, H.; Ablekim, T.; Khan, I.; Persson, K.A.; Zakutayev, A. Wide Band Gap Chalcogenide Semiconductors. *Chem. Rev.* **2020**, *120*, 4007–4055. [CrossRef]
14. Ramamoorthy, C.; Rajendran, V. Synthesis and Characterization of CuS Nanostructures: Structural, Optical, Electrochemical and Photocatalytic Activity by the Hydro/Solvothermal Process. *Int. J. Hydrogen Energy* **2017**, *42*, 26454–26463. [CrossRef]
15. Thongtem, S.; Wichasilp, C.; Thongtem, T. Transient Solid-State Production of Nanostructured CuS Flowers. *Mater. Lett.* **2009**, *63*, 2409–2412. [CrossRef]
16. Justin Raj, C.; Kim, B.C.; Cho, W.J.; Lee, W.G.; Seo, Y.; Yu, K.H. Electrochemical Capacitor Behavior of Copper Sulfide (CuS) Nanoplatelets. *J. Alloys Compd.* **2014**, *586*, 191–196. [CrossRef]
17. Thongtem, T.; Pilapong, C.; Thongtem, S. Large-Scale Synthesis of CuSHexaplates in Mixed Solvents Using a Solvothermal Method. *Mater. Lett.* **2010**, *64*, 111–114. [CrossRef]
18. Salavati-Niasari, M.; Alizadeh, S.; Mousavi-Kamazani, M.; Mir, N.; Rezaei, O.; Ahmadi, E. Surfactant-Free Fabrication of Copper Sulfides (CuS, Cu_2S) via Hydrothermal Method. *J. Clust. Sci.* **2013**, *24*, 1181–1191. [CrossRef]
19. Grozdanov, I.; Najdoski, M. Optical and Electrical Properties of Copper Sulfide Films of Variable Composition. *J. Solid State Chem.* **1995**, *114*, 469–475. [CrossRef]
20. Isac, L.; Popovici, I.; Enesca, A.; Duta, A. Copper Sulfide (CuxS) Thin Films as Possible p-Type Absorbers in 3D Solar Cells. *Energy Procedia* **2010**, *2*, 71–78. [CrossRef]
21. Goel, S.; Chen, F.; Cai, W. Synthesis and Biomedical Applications of Copper Sulfide Nanoparticles: From Sensors to Theranostics. *Small* **2014**, *10*, 631–645. [CrossRef] [PubMed]
22. Deng, C.; Ge, X.; Hu, H.; Yao, L.; Han, C.; Zhao, D. Template-Free and Green Sonochemical Synthesis of Hierarchically Structured CuS Hollow Microspheres Displaying Excellent Fenton-like Catalytic Activities. *CrystEngComm* **2014**, *16*, 2738–2745. [CrossRef]
23. Tanveer, M.; Cao, C.; Ali, Z.; Aslam, I.; Idrees, F.; Khan, W.S.; But, F.K.; Tahir, M.; Mahmood, N. Template Free Synthesis of CuS Nanosheet-Based Hierarchical Microspheres: An Efficient Natural Light Driven Photocatalyst. *CrystEngComm* **2014**, *16*, 5290–5300. [CrossRef]
24. Zhao, B.; Shao, G.; Fan, B.; Zhao, W.; Xie, Y.; Zhang, R. Synthesis of Flower-like CuS Hollow Microspheres Based on Nanoflakes Self-Assembly and Their Microwave Absorption Properties. *J. Mater. Chem. A* **2015**, *3*, 10345–10352. [CrossRef]
25. Zhang, W.; Wen, X.; Yang, S. Synthesis and Characterization of Uniform Arrays of Copper Sulfide Nanorods Coated with Nanolayers of Polypyrrole. *Langmuir* **2003**, *19*, 4420–4426. [CrossRef]
26. Tanveer, M.; Cao, C.; Aslam, I.; Ali, Z.; Idrees, F.; Tahir, M.; Khan, W.S.; Butt, F.K.; Mahmood, A. Effect of the Morphology of CuS upon the Photocatalytic Degradation of Organic Dyes. *RSC Adv.* **2014**, *4*, 63447–63456. [CrossRef]
27. Prakash, A.; Dan, M.; Yu, S.; Wei, S.; Li, Y.; Wang, F.; Zhou, Y. In_2S_3/CuS Nanosheet Composite: An Excellent Visible Light Photocatalyst for H_2 Production from H_2S. *Sol. Energy Mater. Sol. Cells* **2018**, *180*, 205–212. [CrossRef]
28. Sagade, A.A.; Sharma, R. Copper Sulphide (CuxS) as an Ammonia Gas Sensor Working at Room Temperature. *Sens. Actuators B Chem.* **2008**, *133*, 135–143. [CrossRef]
29. Ding, C.; Wang, Z.; Zhong, H.; Zhang, S. Ultrasensitive Chemiluminescence Quantification of Single-Nucleotide Polymorphisms by Using Monobase-Modified Au and CuS Nanoparticles. *Biosens. Bioelectron.* **2010**, *25*, 1082–1087. [CrossRef] [PubMed]
30. Zhang, X.; Wang, G.; Gu, A.; Wei, Y.; Fang, B. CuS Nanotubes for Ultrasensitive Nonenzymatic Glucose Sensors. *Chem. Commun.* **2008**, *45*, 5945–5947. [CrossRef] [PubMed]
31. Wang, Y.; Liu, F.; Ji, Y.; Yang, M.; Liu, W.; Wang, W.; Sun, Q.; Zhang, Z.; Zhao, X.; Liu, X. Controllable Synthesis of Various Kinds of Copper Sulfides (CuS, Cu_7S_4, Cu_9S_5) for High-Performance Supercapacitors. *Dalt. Trans.* **2015**, *44*, 10431–10437. [CrossRef] [PubMed]
32. Myung, Y.; Jang, D.M.; Cho, Y.J.; Kim, H.S.; Park, J.; Kim, J.U.; Choi, Y.; Lee, C.J. Nonenzymatic Amperometric Glucose Sensing of Platinum, Copper Sulfide, and Tin Oxide Nanoparticle-Carbon Nanotube Hybrid Nanostructures. *J. Phys. Chem. C* **2009**, *113*, 1251–1259. [CrossRef]
33. Bo, X.; Bai, J.; Wang, L.; Guo, L. In Situ Growth of Copper Sulfide Nanoparticles on Ordered Mesoporous Carbon and Their Application as Nonenzymatic Amperometric Sensor of Hydrogen Peroxide. *Talanta* **2010**, *81*, 339–345. [CrossRef]
34. Liu, J.; Xue, D. Rapid and Scalable Route to CuS Biosensors: A Microwave-Assisted Cu-Complex Transformation into CuS Nanotubes for Ultrasensitive Nonenzymatic Glucose Sensor. *J. Mater. Chem.* **2011**, *21*, 223–228. [CrossRef]
35. Qiana, L.; Maoa, J.; Tiana, X.; Yuanb, H.; Xiaoa, D. In Situ Synthesis of CuS Nanotubes on Cu Electrode for Sensitive Nonenzymatic Glucose Sensor. *Sens. Actuators B Chem.* **2013**, *176*, 952–959. [CrossRef]
36. Ku, G.; Zhou, M.; Song, S.; Huang, Q.; Hazle, J.; Li, C. Copper Sulfide Nanoparticles as a New Class of Photoacoustic Contrast Agent for Deep Tissue Imaging at 1064 nm. *ACS Nano* **2012**, *6*, 7489–7496. [CrossRef]
37. Tian, Q.; Tang, M.; Sun, Y.; Zou, R.; Chen, Z.; Zhu, M.; Yang, S.; Wang, J.; Wang, J.; Hu, J. Hydrophilic Flower-like Cus Superstructures as an Efficient 980 nm Laser-Driven Photothermal Agent for Ablation of Cancer Cells. *Adv. Mater.* **2011**, *23*, 3542–3547. [CrossRef] [PubMed]

38. Tian, Q.; Jiang, F.; Zou, R.; Liu, Q.; Chen, Z.; Zhu, M.; Yang, S.; Wang, J.; Wang, J.; Hu, J. Hydrophilic Cu_9S_5 Nanocrystals: A Photothermal Agent with a 25.7% Heat Conversion Efficiency for Photothermal Ablation of Cancer Cells in Vivo. *ACS Nano* **2011**, *5*, 9761–9771. [CrossRef] [PubMed]
39. Lakshmanan, S.B.; Zou, X.; Hossu, M.; Ma, L.; Yang, C.; Chen, W. Local Field Enhanced Au/CuS Nanocomposites as Efficient Photothermal Transducer Agents for Cancer Treatment. *J. Biomed. Nanotechnol.* **2012**, *8*, 883–890. [CrossRef] [PubMed]
40. Jung, J.; Jeon, H.J.; Yang, S.W.; Choi, M.; Vidyasagar, D.; Kim, J.H.; Shim, R.B.; Yun, ϒ.; Han, S.; Cho, I.S.; et al. Cost-effective Synthesis of Copper Sulfide Nanoparticles and Flexible Films for Photocatalytic and Antibiotic Applications. *J. Mater. Res. Technol.* **2024**, *28*, 1875–1882. [CrossRef]
41. Al-Hammadi, A.H.; Al-Adhreai, A.A.; Abdulwahab, A.M. An Investigation on the Structural, Morphological, Optical, and Antibacterial Activity of Sr:CuS Nanostructures. *Sci. Rep.* **2024**, *14*, 25169. [CrossRef] [PubMed]
42. Dhasade, S.S.; Patil, J.S.; Kim, J.H.; Han, S.H.; Rath, M.C.; Fulari, V.J. Synthesis of CuS Nanorods Grown at Room Temperature by Electrodeposition Method. *Mater. Chem. Phys.* **2012**, *137*, 353–358. [CrossRef]
43. Mageshwari, K.; Mali, S.S.; Hemalatha, T.; Sathyamoorthy, R.; Patil, P.S. Low Temperature Growth of CuS Nanoparticles by Reflux Condensation Method. *Prog. Solid State Chem.* **2011**, *39*, 108–113. [CrossRef]
44. Huang, J.; Wang, Y.; Gu, C.; Zhai, M. Large Scale Synthesis of Uniform CuS Nanotubes by a Sacrificial Templating Method and Their Application as an Efficient Photocatalyst. *Mater. Lett.* **2013**, *99*, 31–34. [CrossRef]
45. Chen, Y.C.; Shi, J.B.; Wu, C.; Chen, C.J.; Lin, Y.T.; Wu, P.F. Fabrication and Optical Properties of CuS Nanowires by Sulfuring Method. *Mater. Lett.* **2008**, *62*, 1421–1423. [CrossRef]
46. Basu, M.; Nazir, R.; Fageria, P.; Pande, S. Construction of CuS/Au Heterostructure through a Simple Photoreduction Route for Enhanced Electrochemical Hydrogen Evolution and Photocatalysis. *Sci. Rep.* **2016**, *6*, 34738. [CrossRef]
47. Basu, M.; Sinha, A.K.; Pradhan, M.; Sarkar, S.; Negishi, Y.; Govind; Pal, T. Evolution of Hierarchical Hexagonal Stacked Plates of CuS from Liquid-Liquid Interface and Its Photocatalytic Application for Oxidative Degradation of Different Dyes under Indoor Lighting. *Environ. Sci. Technol.* **2010**, *44*, 6313–6318. [CrossRef] [PubMed]
48. Rajendran, V.; Gajendiran, J. Nonionic Surfactant Poly(ethane 1,2-Diol)-400 Assisted Solvothermal Synthesis of Copper Monosulfide (CuS) Nanoplates and Their Structural, Topographical, Optical and Luminescent Properties. *Mater. Sci. Semicond. Process.* **2015**, *36*, 92–95. [CrossRef]
49. Mousavi-Kamazani, M.; Zarghami, Z.; Salavati-Niasari, M. Facile and Novel Chemical Synthesis, Characterization, and Formation Mechanism of Copper Sulfide (Cu_2S, Cu_2S/CuS, CuS) Nanostructures for Increasing the Efficiency of Solar Cells. *J. Phys. Chem. C* **2016**, *120*, 2096–2108. [CrossRef]
50. Ain, N.; Nasir, J.A.; Khan, Z.; Butlerb, I.S.; Rehman, Z. Copper sulfide nanostructures: Synthesis and biological applications. *RSC Adv.* **2022**, *12*, 7550–7567. [CrossRef]
51. Kumar, P.; Agrawal, N.; Choudhary, S.D.; Gautam, A.K. Highly-Efficient Solution Processed Yellow Organic Light Emitting Diode with Tungsten Trioxide Hole Injection/Transport Layer. *IEEE Trans. Nanotechnol.* **2020**, *19*, 61–66. [CrossRef]
52. Guo, K.; Tang, Z.; Chou, X.; Pan, S.; Wan, C.; Xue, T.; Ding, L.; Wang, X.; Huang, J.; Zhang, F.; et al. Printable Organic Light-Emitting Diodes for next-Generation Visible Light Communications: A Review. *Adv. Photonics Nexus* **2023**, *2*, 044001. [CrossRef]
53. Mohan, V.; Gautam, A.K.; Choudhary, S.D.; Mariam Bee, M.K.; Puviarasi, R.; Saranya, S.; Agrawal, N. Enhanced Performance Organic Light Emitting Diode with CuI:CuPC Composite Hole Transport Layer. *IEEE Trans. Nanotechnol.* **2020**, *19*, 699–703. [CrossRef]
54. Liu, B.; Altintas, Y.; Wang, L.; Shendre, S.; Sharma, M.; Sun, H.; Mutlugun, E.; Demir, H.V. Record High External Quantum Efficiency of 19.2% Achieved in Light-Emitting Diodes of Colloidal Quantum Wells Enabled by Hot-Injection Shell Growth. *Adv. Mater.* **2020**, *32*, 9–10. [CrossRef] [PubMed]
55. Yang, J.H.; Jang, G.P.; Kim, S.Y.; Chae, Y.B.; Lee, K.H.; Moon, D.G.; Kim, C.K. Highly Efficient All-Solution-Processed Quantum Dot Light-Emitting Diodes Using MoOx Nanoparticle Hole Injection Layer. *Nanomaterials* **2023**, *13*, 2324. [CrossRef]
56. Pozov, S.M.; Ioakeimidis, A.; Papadas, I.T.; Sun, C.; Chrusou, A.Z.; Bradley, D.D.C.; Choulis, S.A. Bottom Contact Metal Oxide Interface Modification Improving the Efficiency of Organic Light Emitting Diodes. *Materials* **2020**, *13*, 5082. [CrossRef] [PubMed]
57. So, F.; Kondakov, D. Degradation Mechanisms in Small-Molecule and Polymer Organic Light-Emitting Diodes. *Adv. Mater.* **2010**, *22*, 3762–3777. [CrossRef]
58. De Jong, M.P.; Van Ijzendoorn, L.J.; De Voigt, M.J.A. Stability of the Interface between Indium-Tin-Oxide and Poly(3,4-ethylenedioxythiophene)/Poly(styrenesulfonate) in Polymer Light-Emitting Diodes. *Appl. Phys. Lett.* **2000**, *77*, 2255–2257. [CrossRef]
59. Han, T.H.; Song, W.; Lee, T.W. Elucidating the Crucial Role of Hole Injection Layer in Degradation of Organic Light-Emitting Diodes. *ACS Appl. Mater. Interfaces* **2015**, *7*, 3117–3125. [CrossRef]
60. Zhang, X.; You, F.; Zheng, Q.; Zhang, Z.; Cai, P.; Xue, X.; Xiong, J.; Zhang, J. Solution-Processed MoO_x Hole Injection Layer towards Efficient Organic Light-Emitting Diode. *Org. Electron.* **2016**, *39*, 43–49. [CrossRef]

61. Shi, S.; Sadhu, V.; Moubah, R.; Schmerber, G.; Bao, Q.; Silva, S.R.P. Solution-Processable Graphene Oxide as an Efficient Hole Injection Layer for High Luminance Organic Light-Emitting Diodes. *J. Mater. Chem. C* **2013**, *1*, 1708–1712. [CrossRef]
62. Kubelka, P.; Munk, F. Ein Beitrag Zur Optik Der Farbanstriche. *Z. Techn. Phys.* **1931**, *12*, 593–601.
63. Ioakeimidis, A.; Kottaras, A.; Karageorgopoulos, D.; Christia, E.; Sakkopoulos, S.; Vitoratos, E.; Choulis, S.A.; Papadas, I.T. Conductivity Transport Mechanisms of Solution-Processed Spinel Nickel Cobaltite-Based Hole Transporting Layers and Its Implementation as Charge Selective Contact in Organic Photovoltaics. *Environ. Sci. Proc.* **2023**, *26*, 63. [CrossRef]
64. Papadas, I.T.; Ioakeimidis, A.; Armatas, G.S.; Choulis, S.A. Low-Temperature Combustion Synthesis of a Spinel $NiCo_2O_4$ Hole Transport Layer for Perovskite Photovoltaics. *Adv. Sci.* **2018**, *5*, 1701029. [CrossRef] [PubMed]
65. Ioakeimidis, A.; Papadas, I.T.; Tsikritzis, D.; Armatas, G.S.; Kennou, S.; Choulis, S.A. Enhanced Photovoltaic Performance of Perovskite Solar Cells by Co-Doped Spinel Nickel Cobaltite Hole Transporting Layer. *APL Mater.* **2019**, *7*, 021101. [CrossRef]
66. Papadas, I.T.; Kota, S.S.; Kanatzidis, M.G.; Armatas, G.S. Templated Assembly of $BiFeO_3$ Nanocrystals into 3D Mesoporous Networks for Catalytic Applications. *Nanoscale* **2015**, *7*, 5737–5743. [CrossRef]
67. Bowmaker, G.A.; Hanna, J.V.; Pakawatchai, C.; Skelton, B.W.; Thanyasirikul, Y.; White, A.H. Crystal Structures and Vibrational Spectroscopy of Copper(l) Thiourea Complexes. *Inorg. Chem.* **2009**, *48*, 350–368. [CrossRef]
68. Bordwell, F.G.; Ji, G.Z. Effects of Structural Changes on Acidities and Homolytic Bond Dissociation Energies of the H–N Bonds in Amidines, Carboxamides, and Thiocarboxamides. *J. Am. Chem. Soc.* **1991**, *113*, 8398–8401. [CrossRef]
69. Liu, F.; Shen, S.; Zhou, F.; Song, N.; Wen, X.; Stride, J.A.; Sun, K.; Yan, C.; Hao, X. Kesterite Cu_2ZnSnS_4 Thin Film Solar Cells by a Facile DMF-Based Solution Coating Process. *J. Mater. Chem. C* **2015**, *3*, 10783–10792. [CrossRef]
70. Ki, W.; Hillhouse, H.W. Earth-Abundant Element Photovoltaics Directly from Soluble Precursors with High Yield Using a Non-Toxic Solvent. *Adv. Energy Mater.* **2011**, *1*, 732–735. [CrossRef]
71. Todorov, T.; Hillhouse, H.W.; Aazou, S.; Sekkat, Z.; Vigil-Galán, O.; Deshmukh, S.D.; Agrawal, R.; Bourdais, S.; Valdés, M.; Arnou, P.; et al. Solution-Based Synthesis of Kesterite Thin Film Semiconductors. *J. Phys. Energy* **2020**, *2*, 012003. [CrossRef]
72. Wu, H.; Or, V.W.; Gonzalez-Calzada, S.; Grassian, V.H. CuS Nanoparticles in Humid Environments: Adsorbed Water Enhances the Transformation of CuS to $CuSO_4$. *Nanoscale* **2020**, *12*, 19350–19358. [CrossRef]
73. Zhao, Y.; Pan, H.; Lou, Y.; Qiu, X.; Zhu, J.; Burda, C. Plasmonic $Cu_{2-X}S$ Nanocrystals: Optical and Structural Properties of Copper-Deficient Copper(I) Sulfides. *J. Am. Chem. Soc.* **2009**, *131*, 4253–4261. [CrossRef]
74. Ravele, M.P.; Oyewo, O.A.; Onwudiwe, D.C. Controlled Synthesis of CuS and Cu_9S_5 and Their Application in the Photocatalytic Mineralization of Tetracycline. *Catalysts* **2021**, *11*, 899. [CrossRef]
75. Ayodhya1, D.; Veerabhadram, G. Preparation, Characterization, Photocatalytic, Sensing and Antimicrobial Studies of Calotropis gigantea Leaf Extract Capped CuS NPs by a Green Approach. *J. Inorg. Organomet. Polym.* **2017**, *27*, 215–230. [CrossRef]
76. Lei, H.; Fang, G.; Cheng, F.; Ke, W.; Qin, P.; Song, Z.; Zheng, Q.; Fan, X.; Huang, H.; Zhao, X. Enhanced Efficiency in Organic Solar Cells via in situ Fabricated P-Type Copper Sulfide as the Hole Transporting Layer. *Sol. Energy Mater. Sol. Cells* **2014**, *128*, 77–84. [CrossRef]